Supporting Information

Differences in Nanoparticle Uptake in Transplanted and Autochthonous Models of Pancreatic Cancer

Zhimin Tao,[1,*] Mandar Deepak Muzumdar,[1,2,3,4*] Alexandre Detappe,[1,2,3] Xing Huang,[1] Eric S. Xu,[1] Yingjie Yu,[1] Tarek H. Mouhieddine,[2,3] Haiqin Song,[1] Tyler Jacks,[1] and P. Peter Ghoroghchian[1,2,3,#]

1. Koch Institute for Integrative Cancer Research at MIT, 500 Main Street, Cambridge, MA 02139, USA
2. Dana Farber Cancer Institute, 450 Brookline Avenue, Boston, MA 02215, USA
3. Harvard Medical School, 25 Shattuck Street, Boston, MA 02115, USA
4. Yale University School of Medicine, 333 Cedar Street, New Haven, CT 06510, USA

* Denotes equal author contribution

To whom correspondence should be addressed:

P. Peter Ghoroghchian, M.D., Ph.D.
Charles W. and Jennifer C. Johnson Clinical Investigator
Koch Institute for Integrative Cancer Research
Massachusetts Institute of Technology
77 Massachusetts Avenue, 76-261F
Cambridge, MA 02139, USA
(617) 252-1163
ppg@mit.edu

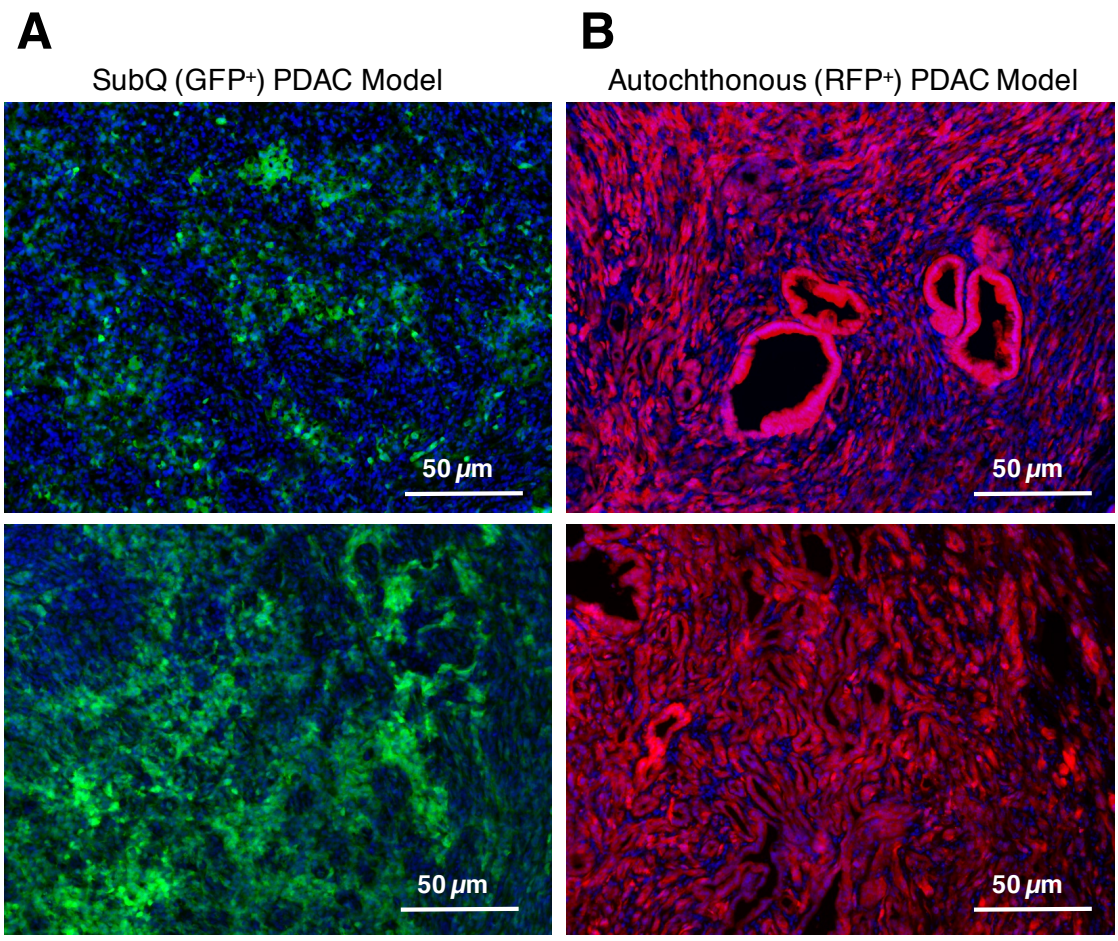

Figure S1: Fluorescence micrographs of tumors from additional mice (2 animals per model) illustrating differences in tumor microarchitecture. (A) Subcutaneous green fluorescent protein (GFP)-expressing pancreatic tumor allografts, consisting of B22 *Kras;p53* mutant murine PDAC cells (green) implanted in the flanks of nude mice. (B) Tumors from TdTomato red fluorescence protein (RFP)-expressing autochthonous *KPC* mice, generating primary pancreatic PDAC cells (red). The dense desmoplastic stroma may be visualized by labeled cells (DAPI; blue) that do not have additional fluorescence protein expression in the cytoplasm. Micrographs taken of tumors from two-separate mice are displayed for each group. Scale bar = 50 μm.

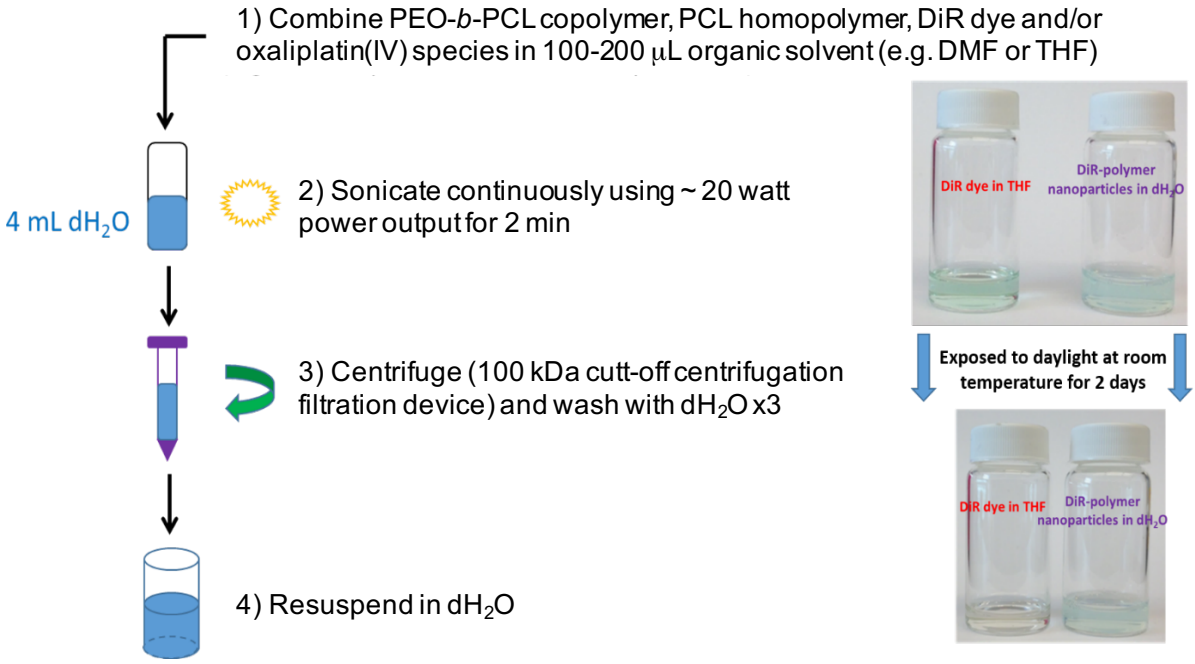

Scheme S1. Generation of PEO-*b*-PCL-based nanoparticles. The synthesis of PEO-*b*-PCL-based nanoparticles commenced by first dissolving a given PEO-*b*-PCL diblock copolymer composition, a homopolymer of PCL, the near-infrared fluorophore DiR, and/or the lipophilic oxaliplatin(IV) prodrug in organic solvent (THF for nanospheres or DMF for eventual generation of nanoscale worm-like micelles). The organic solvent (100-200 μL) was then dispersed in a larger aqueous volume (*e.g.*, 4 mL of dH_2O) under continuous sonication. The formed nanoparticles were subsequently washed with dH_2O and concentrated by centrifugation filtration (x3 cycles) to remove residual organic solvent. The nanoparticles were finally suspended in fresh aqueous solution prior to further *in vitro* or *in vivo* experimentation. The inset photographs (right) visually depict that the DiR fluorophore remains grossly suspended in nanoparticle suspensions (light blue) even after 48 h of exposure to daylight and at room temperature; DiR in organic solution (*e.g.*, THF) is rapidly degraded under the same conditions, resulting in a clear solution.

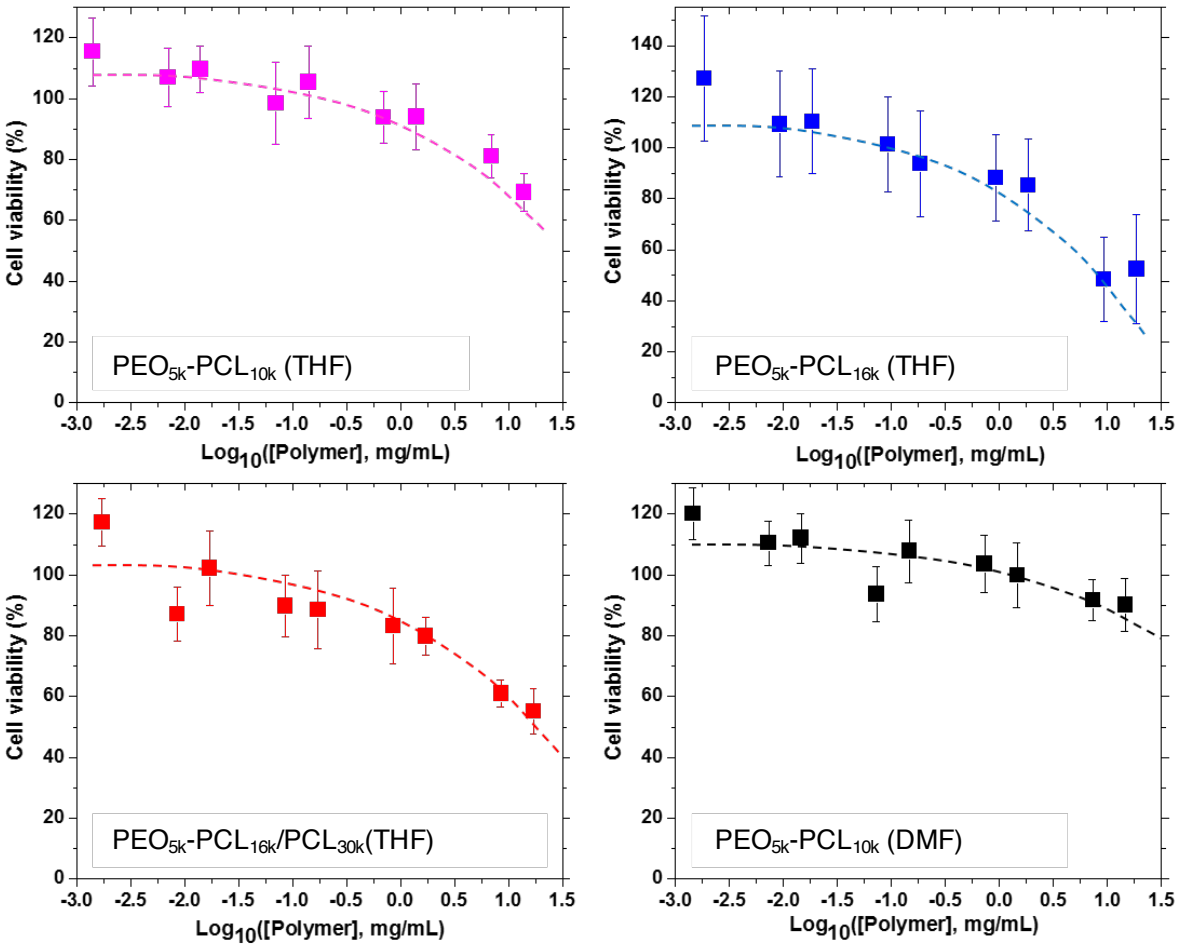

Figure S2. ***In vitro*** **cytotoxicity of various PEO-*b*-PCL-based nanoparticles differing in size and shape as examined with cultured B22 murine PDAC cells.** The CellTiterGlo bioluminescence cell viability assay was performed after 72 h of exposure of B22 cells (plated at 5,000 cells per well) with different concentrations of unloaded PEO-*b*-PCL-based nanoparticles (n=6 technical replicates per nanoparticle formulation). The results were normalized to that of untreated cells and were plotted as a function of increasing polymer concentration for each of the nanoparticle formulations.

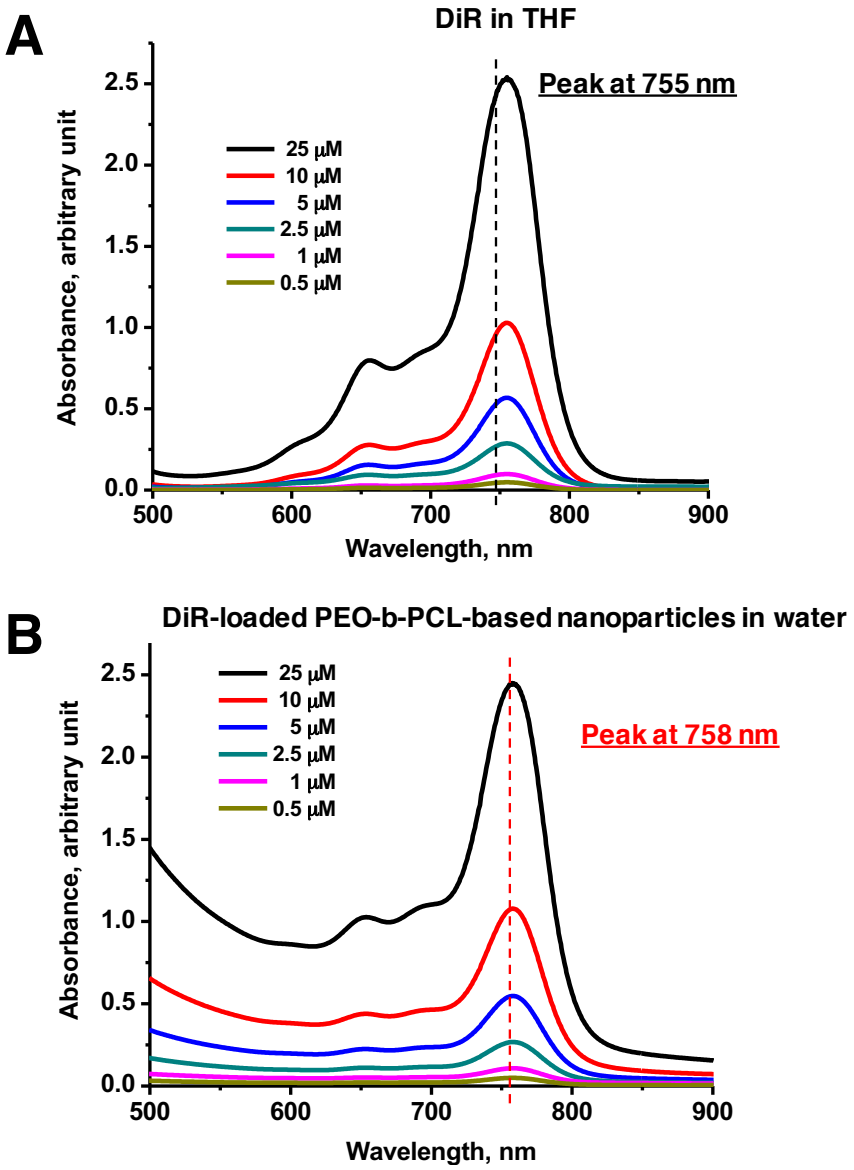

Figure S3. Characterization of the solubility of DiR in the polymeric environment of PEO-*b*-PCL-based nanoparticles. UV-Vis measurements of the absorbance of different concentrations of DiR in (A) THF (organic solvent) and in (B) aqueous suspensions of PEO-*b*-PCL-based nanoparticles in water (*i.e.*, 100 nm-diameter nanospheres comprised of PEO_{5k}-PCL_{16k}). A slight bathochromic shift in the peak absorbance wavelength was visualized and was consistent with the results observed in previous investigations that have incorporated this fluorophore within spherical PEO-*b*-PCL-based nanoparticles [1].

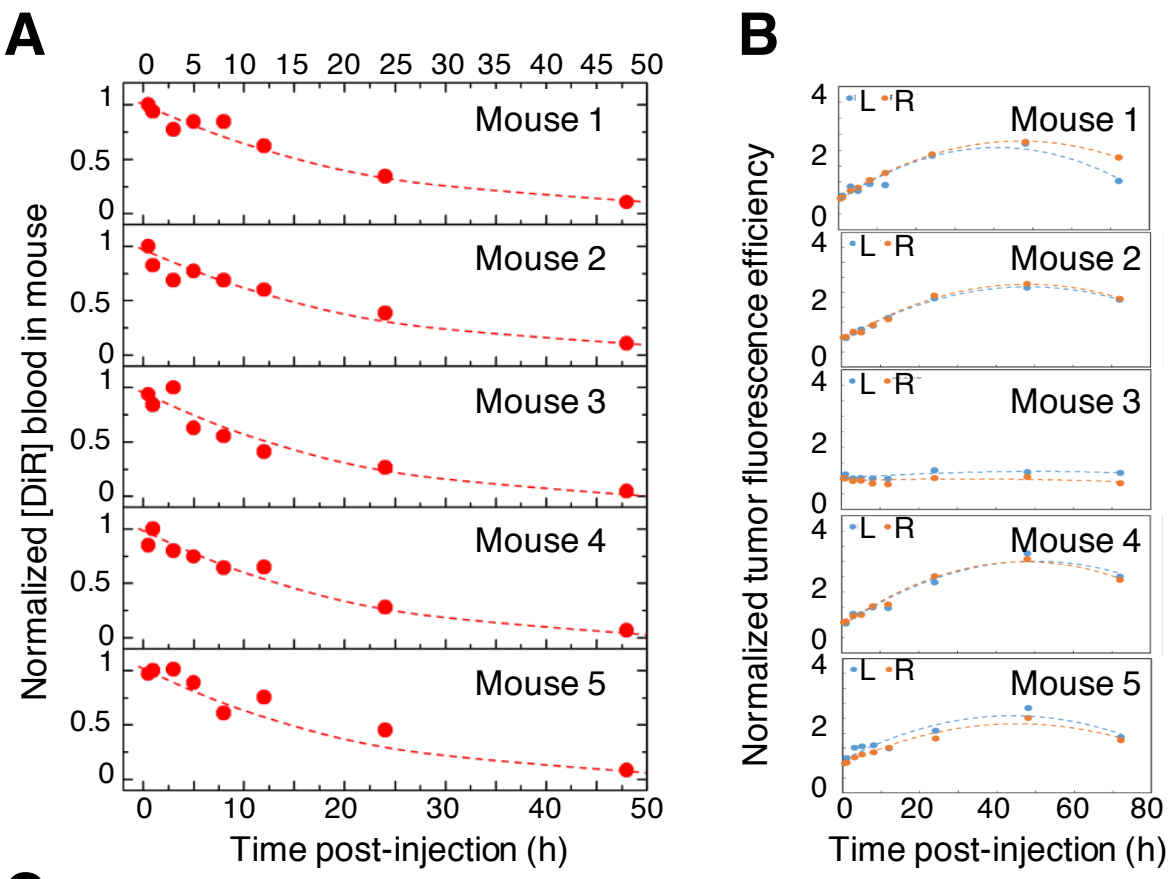

C

Tumor	R^2	a	b	c	Calculated time to reach maximal tumor accumulation (h)	Calculated maximal tumor accumulation (fold)
1# left	0.921	-0.001	0.0816	0.9196	40.8	2.6
1# right	0.999	-0.0008	0.0773	0.9788	48.3	2.8
2# left	0.996	-0.0008	0.0729	0.9184	45.6	2.6
2# right	0.987	-0.0008	0.0777	0.8995	48.6	2.8
3# left	0.548	-0.00009	0.0086	1.0023	47.8	1.2
3# right	0.084	-0.00005	0.0035	0.9188	35.0	1.0
4# left	0.958	-0.0008	0.0847	0.881	52.9	3.1
4# right	0.983	-0.0009	0.0877	0.8985	48.7	3.0
5# left	0.872	-0.0008	0.0679	1.0893	42.4	2.5
5# right	0.948	-0.0007	0.06	0.9582	42.9	2.2

Figure S4. Pharmacokinetics and tumor accumulation of 70 nm-diameter nanospheres comprised of PEO_{5k}-PCL_{10k} (THF) and encapsulating DiR as assessed in nude mice bearing SQ pancreatic tumors. At the indicated time points, 15 μL of blood were withdrawn from each mouse (n=5 mice that were similarly administered the nanoparticles via IV-tail vein injection) by retro-orbital venipuncture, using heparinized microcapillary tubes; this was followed by simultaneously fluorescence readings of all samples (n = 5 capillary tubes) at each time point, using the IVIS instrument. Radiant efficiency values were converted to [DiR] in mouse blood; they were normalized to the highest values obtained from the initial readings immediately after nanoparticle administration. (A) [DiR] in the blood of each mouse was plotted over time to obtain the blood circulatory half-life ($t_{1/2}$) of the nanoparticle formulation. (B) *In vivo* fluorescence

readings from tumors implanted on both the left and right flanks of each animal, which were obtained by co-localization of bioluminescence signals emanating from the tumor areas. The fluorescence radiant efficiency values were monitored at different time points, were normalized to their starting values, and were plotted over time. The dotted line represents the mathematic fit of a 2^{nd}-order polynomial function ($Y= a*X^2+b*X+c$). (C) Summary of all parametric values from the mathematic function described in (B).

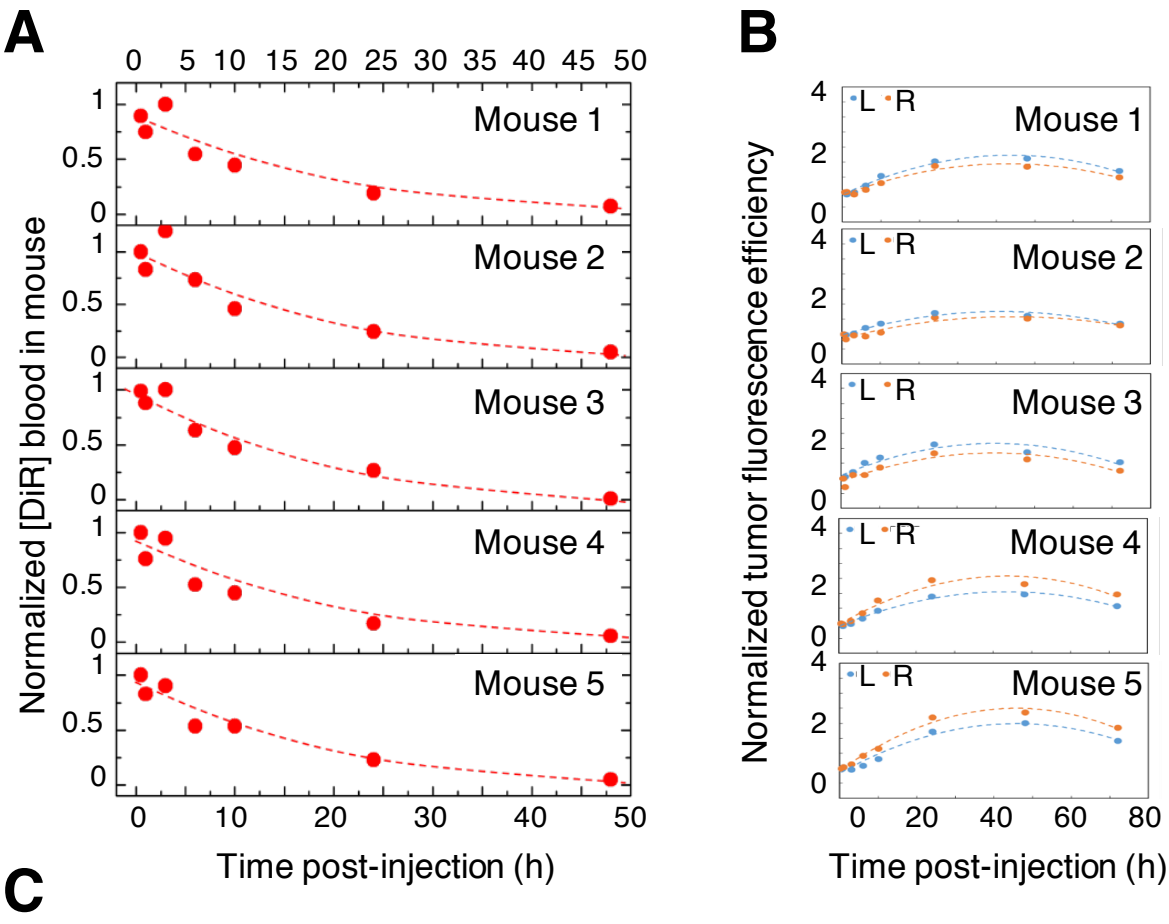

C

Tumor	R^2	a	b	c	Calculated time to reach maximal tumor accumulation (h)	Calculated maximal tumor accumulation (fold)
1# left	0.976	-0.0007	0.0604	0.9105	43.1	2.2
1# right	0.945	-0.0006	0.0485	0.8964	40.4	1.9
2# left	0.942	-0.0005	0.0378	0.9703	37.8	1.7
2# right	0.887	-0.0004	0.0331	0.8446	41.4	1.5
3# left	0.873	-0.0007	0.0538	1.0956	38.4	2.1
3# right	0.863	-0.0006	0.0484	0.8884	40.3	1.9
4# left	0.978	-0.0006	0.053	0.9021	44.2	2.1
4# right	0.944	-0.0009	0.0742	0.9595	41.2	2.5
5# left	0.962	-0.0008	0.0725	0.8302	45.3	2.5
5# right	0.986	-0.001	0.0907	0.9257	45.4	3.0

Figure S5. Pharmacokinetics and tumor accumulation of 100 nm-diameter nanospheres comprised of PEO_{5k}-PCL_{16k} (THF) and encapsulating DiR as assessed in nude mice bearing SQ pancreatic tumors. At the indicated time points, 15 μL of blood were withdrawn from each mouse (n=5 mice that were similarly administered the nanoparticles via IV-tail vein injection) by retro-orbital venipuncture, using heparinized microcapillary tubes; this was followed by simultaneously fluorescence readings of all samples (n = 5 capillary tubes) at each time point, using the IVIS instrument. Radiant efficiency values were converted to [DiR] in mouse blood; they were normalized to the highest values obtained from the initial readings immediately after

nanoparticle administration. (A) [DiR] in the blood of each mouse was plotted over time to obtain the blood circulatory half-life ($t_{1/2}$) of the nanoparticle formulation. (B) *In vivo* fluorescence readings from tumors implanted on both the left and right flanks of each animal, which were obtained by co-localization of bioluminescence signals emanating from the tumor areas. The fluorescence radiant efficiency values were monitored at different time points, were normalized to their starting values, and were plotted over time. The dotted line represents the mathematic fit of a 2^{nd}-order polynomial function ($Y= a*X^2+b*X+c$). (C) Summary of all parametric values from the mathematic function described in (B).

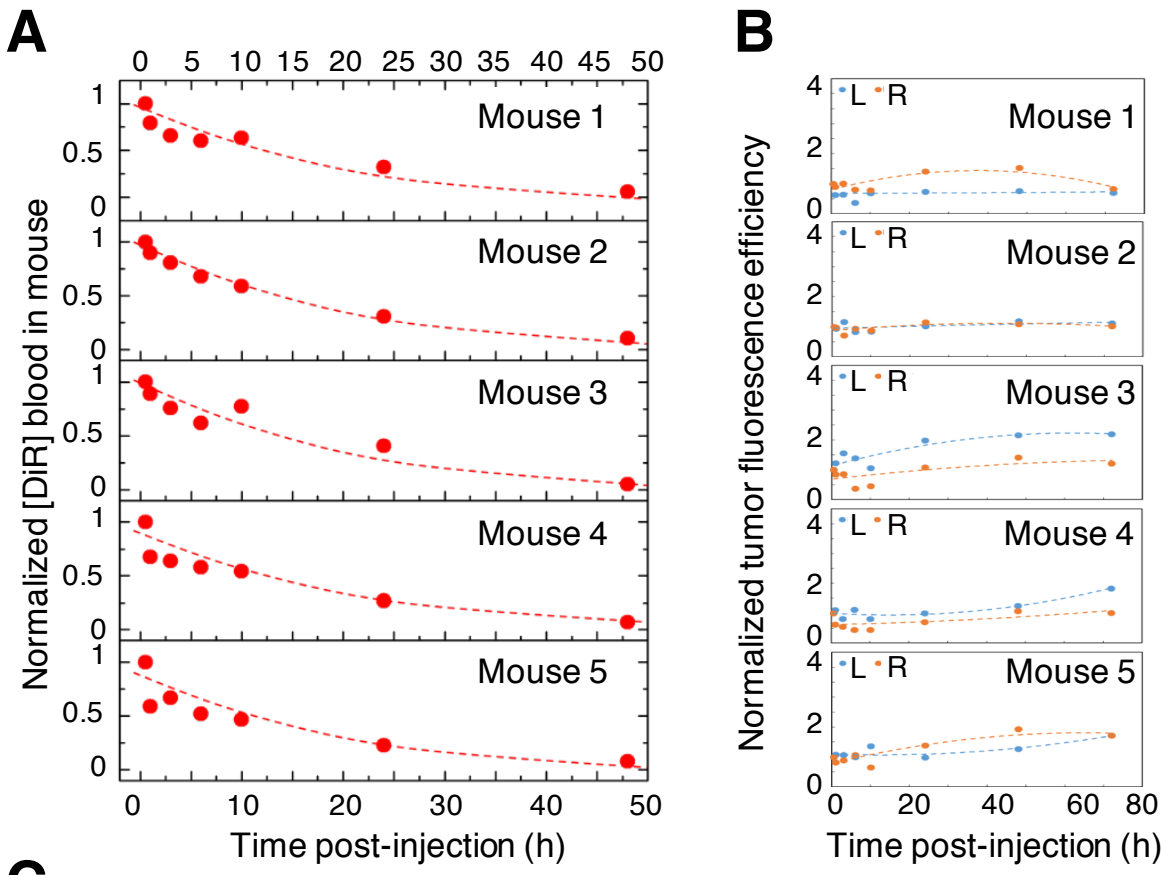

C

Tumor	R^2	a	b	c	Calculated time to reach maximal tumor accumulation (h)	Calculated maximal tumor accumulation (fold)
1# left	0.011	0.000005	0.0003	0.6812	-30	0.7
1# right	0.636	-0.0005	0.0341	0.8025	34.1	1.4
2# left	0.286	-0.000007	0.0033	0.9536	235.7	1.3
2# right	0.414	-0.0001	0.0108	0.8781	54	1.2
3# left	0.811	-0.0003	0.0354	1.1375	59	2.2
3# right	0.451	-0.00009	0.015	0.6867	83.3	1.3
4# left	0.884	0.0003	0.0083	1.0019	-13.8	0.9
4# right	0.415	0.00005	0.0029	0.6172	-29	0.6
5# left	0.750	0.0002	-0.0043	1.0916	10.8	1.1
5# right	0.808	-0.0002	0.0314	0.7853	78.5	2.0

Figure S6. Pharmacokinetics and tumor accumulation of 300 nm-diameter nanospheres comprised of PEO_{5k}-PCL_{16k} /PCL_{30k} (THF) and encapsulating DiR as assessed in nude mice bearing SQ pancreatic tumors. At the indicated time points, 15 μL of blood were withdrawn from each mouse (n=5 mice that were similarly administered the nanoparticles via IV-tail vein injection) by retro-orbital venipuncture, using heparinized microcapillary tubes; this was followed by simultaneously fluorescence readings of all samples (n = 5 capillary tubes) at each time point, using the IVIS instrument. Radiant efficiency values were converted to [DiR] in mouse blood; they were normalized to the highest values obtained from the initial readings immediately after nanoparticle administration. (A) [DiR] in the blood of each mouse was plotted over time to obtain the blood circulatory half-life ($t_{1/2}$) of the nanoparticle formulation. (B) *In vivo* fluorescence

readings from tumors implanted on both the left and right flanks of each animal, which were obtained by co-localization of bioluminescence signals emanating from the tumor areas. The fluorescence radiant efficiency values were monitored at different time points, were normalized to their starting values, and were plotted over time. The dotted line represents the mathematic fit of a 2^{nd}-order polynomial function ($Y= a*X^2+b*X+c$). (C) Summary of all parametric values from the mathematic function described in (B).

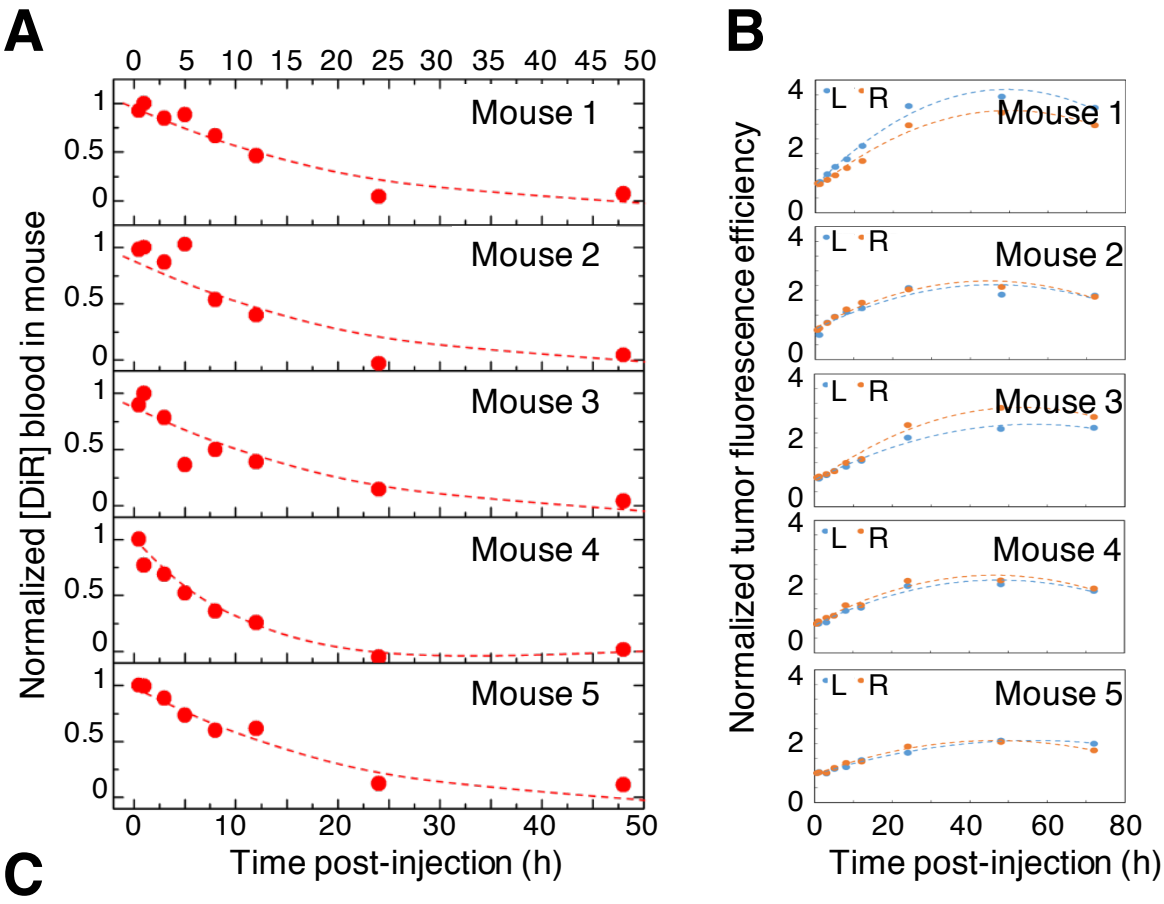

Tumor	R^2	a	b	c	Calculated time to reach maximal tumor accumulation (h)	Calculated maximal tumor accumulation (fold)
1# left	0.986	-0.0013	0.1319	0.9301	50.7	4.3
1# right	0.986	-0.001	0.1052	0.8294	52.6	3.6
2# left	0.890	-0.0007	0.0655	1.0249	46.8	2.6
2# right	0.964	-0.0008	0.071	1.0706	44.4	2.6
3# left	0.986	-0.0006	0.0669	0.9096	55.8	2.8
3# right	0.984	-0.0009	0.0945	0.8458	52.5	3.3
4# left	0.971	-0.0007	0.0645	0.9405	46.1	2.4
4# right	0.964	-0.0008	0.0706	0.999	44.1	2.6
5# left	0.989	-0.0004	0.041	0.9473	51.3	2.0
5# right	0.984	-0.0005	0.0493	0.9504	49.3	2.2

Figure S7. Pharmacokinetics and tumor accumulation of 100 nm-diameter worm-like micelles comprised of PEO_{5k}-PCL_{10k} (DMF) and encapsulating DiR as assessed in nude mice bearing SQ pancreatic tumors. At the indicated time points, 15 μL of blood were withdrawn from each mouse (n=5 mice that were similarly administered the nanoparticles via IV-tail vein injection) by retro-orbital venipuncture, using heparinized microcapillary tubes; this was followed by simultaneously fluorescence readings of all samples (n = 5 capillary tubes) at each time point, using the IVIS instrument. Radiant efficiency values were converted to [DiR] in mouse blood; they were normalized to the highest values obtained from the initial readings immediately after nanoparticle administration. (A) [DiR] in the blood of each mouse was plotted over time to obtain the blood circulatory half-life ($t_{1/2}$) of the nanoparticle formulation. (B) *In vivo* fluorescence

readings from tumors implanted on both the left and right flanks of each animal, which were obtained by co-localization of bioluminescence signals emanating from the tumor areas. The fluorescence radiant efficiency values were monitored at different time points, were normalized to their starting values, and were plotted over time. The dotted line represents the mathematic fit of a 2^{nd}-order polynomial function ($Y= a*X^2+b*X+c$). (C) Summary of all parametric values from the mathematic function described in (B).

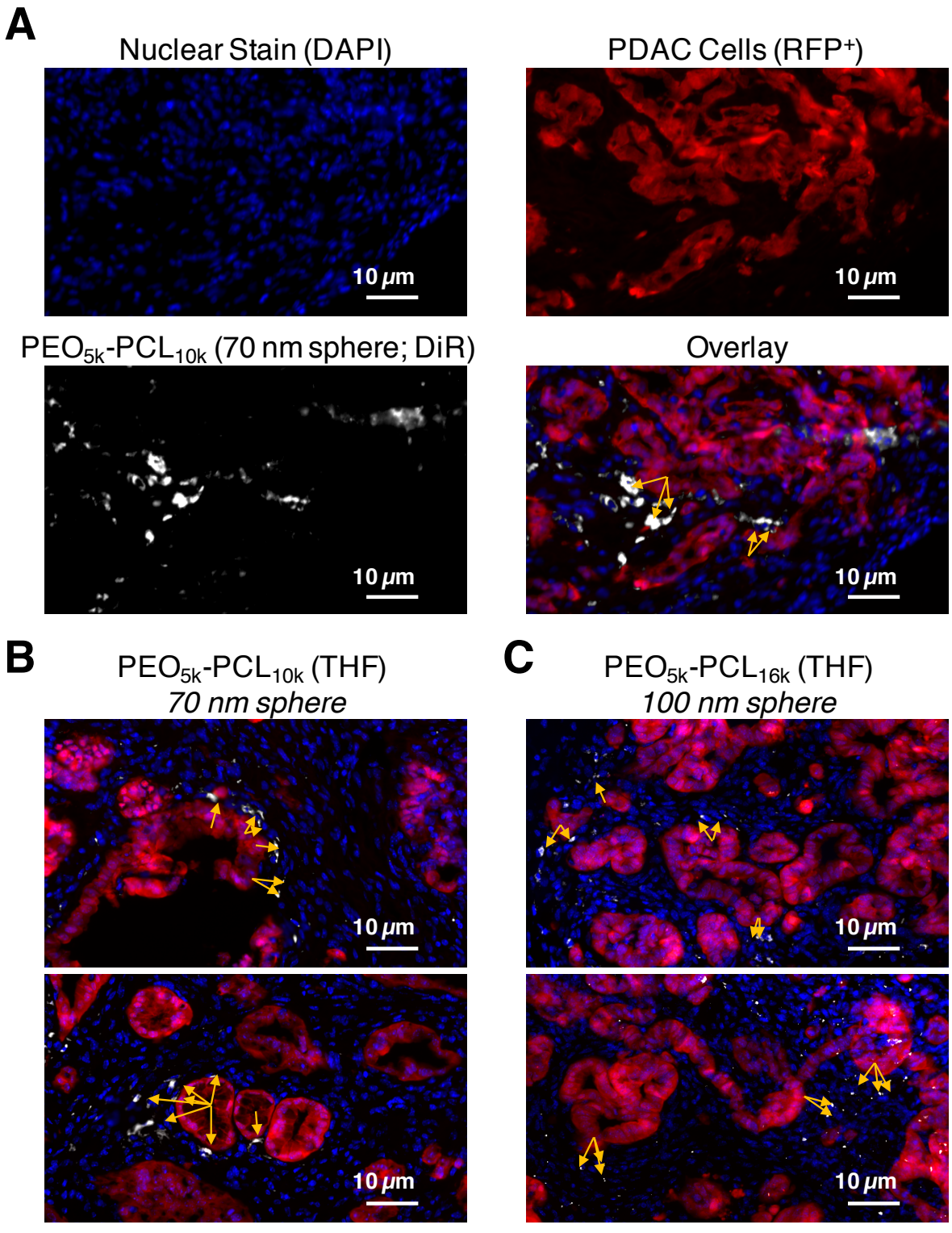
A
Nuclear Stain (DAPI)
PDAC Cells (RFP+)
10 μm
10 μm
PEO5k-PCL10k (70 nm sphere; DiR)
Overlay
10 μm
10 μm
B
PEO5k-PCL10k (THF)
70 nm sphere
C
PEO5k-PCL16k (THF)
100 nm sphere
10 μm
10 μm
10 μm
10 μm

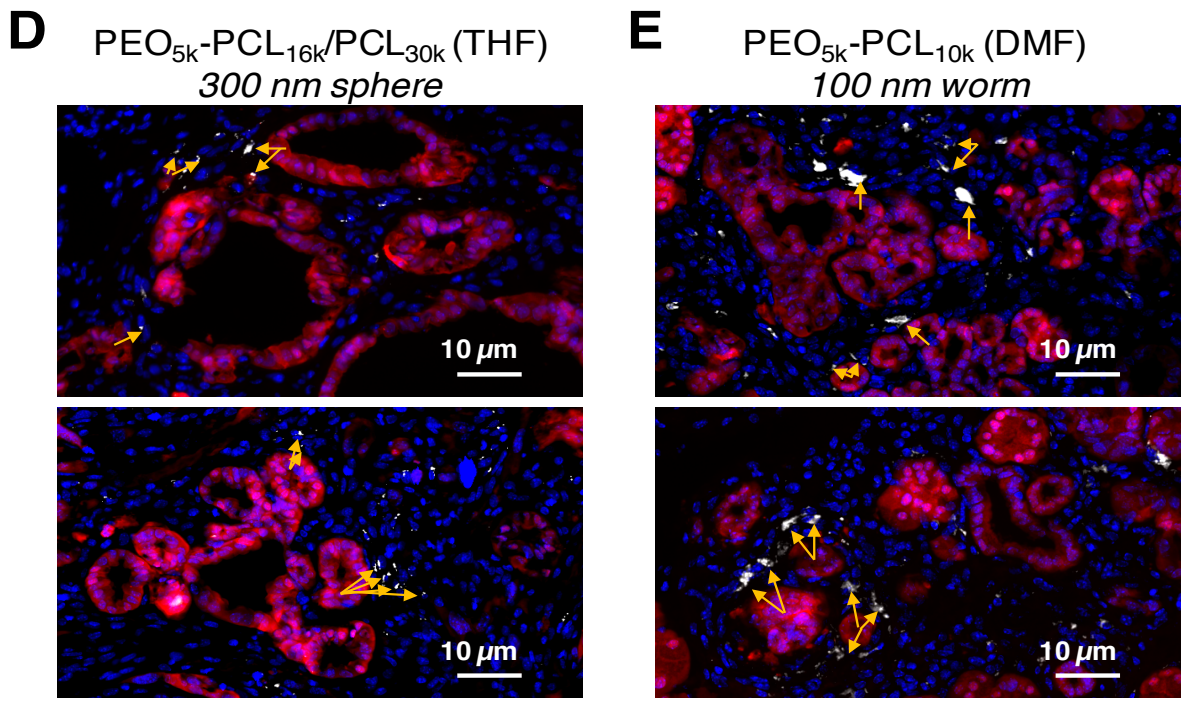

Figure S8: Fluorescence micrographs of TdTomato red fluorescence protein (RFP)-expressing autochthonous pancreatic tumors from *KPC* mice that were administered different nanoparticle formulations. (A) Images taken in different fluorescence channels from a tumor section of a mouse that had been sacrificed at 24 h after administration of DiR-labeled 70 nm-diameter PEO-*b*-PCL-based nanospheres via IV (tail-vein) injection. Cell nuclei are stained with DAPI (blue); the PDAC cells may be visualized via their RFP expression (red); and, the nanoparticles are detected via the near-infrared fluorescence of DiR (white), enabling independent tracking and colocalization of each species in an overlay image; note that the dense desmoplastic stroma is evident by labeled cells (DAPI; blue) that do not have additional fluorescence protein expression in the cytoplasm. (B-E) Overlay images generated via analogous multi-channel imaging (DAPI, RFP, DiR) of tumors taken from additional RFP-expressing autochthonous pancreatic tumors in *KPC* mice that had been administered DiR-labeled 70, 100, or 300 nm-diameter PEO-*b*-PCL-based nanospheres or 100 nm-length PEO-*b*-PCL-based nanoworms via IV injection. Micrographs taken of tumors from two-separate mice are displayed for each group. Scale bar = 10 μm.

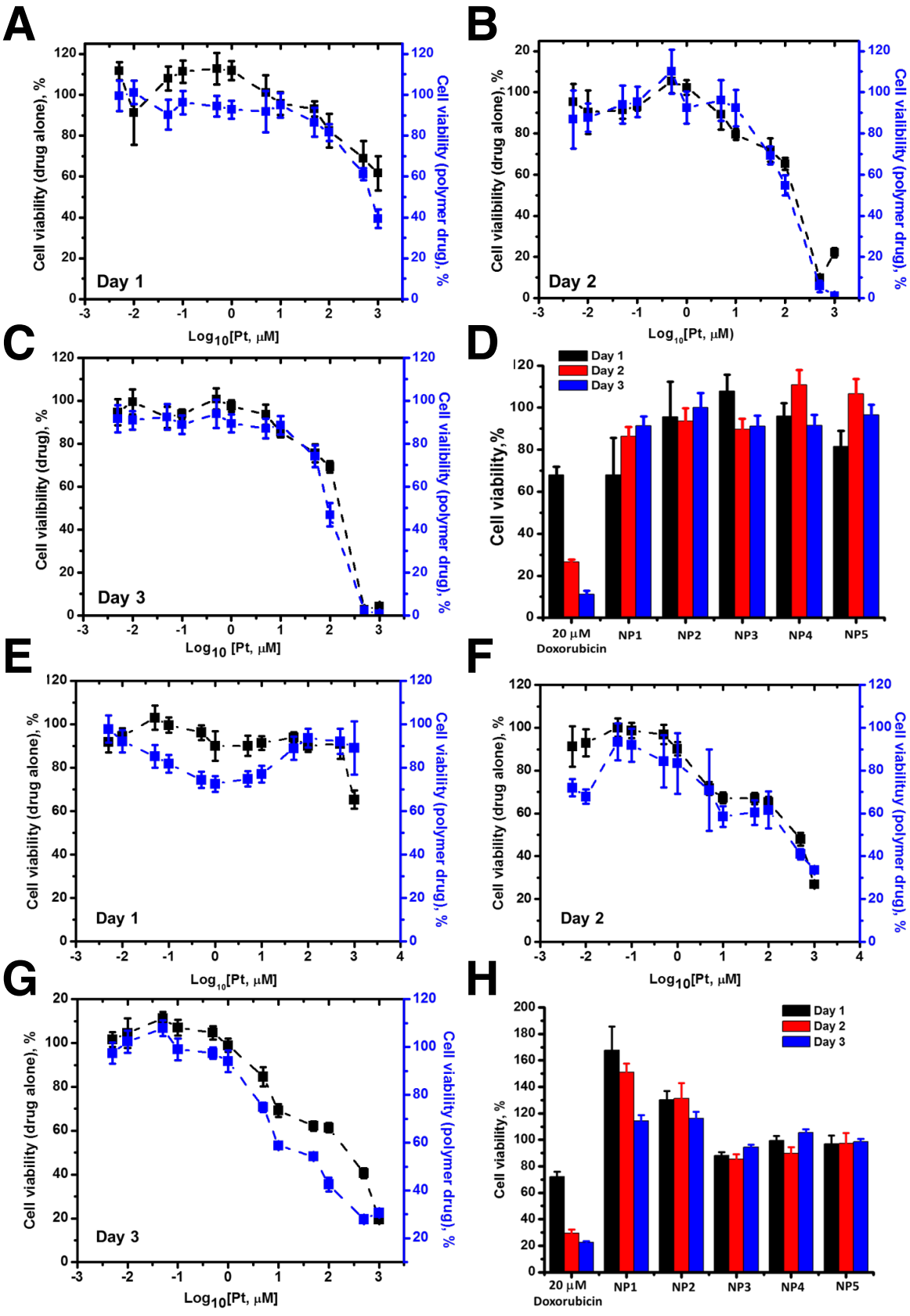
A
Cell viability (drug alone), %
Cell viability (polymer drug), %
Day 1
Log10[Pt, μM]
B
Day 2
C
Day 3
D
Day 1
Day 2
Day 3
Cell viability, %
20 μM Doxorubicin
NP1
NP2
NP3
NP4
NP5
E
Day 1
F
Day 2
G
Day 3
H
Day 1
Day 2
Day 3

Figure S9. Cytotoxicity of oxaliplatin-loaded PEO_{5k}-PCL_{10k}-based worm-like micelles versus free oxaliplatin on murine and human PDAC cells. The CellTiterGlo bioluminescence cell viability assay was performed after (A) 1 day, (B) 2 day or (C) 3 days of continuous exposure of B22 cells (5,000 cells per well) with different concentrations of oxaliplatin(IV)-loaded PEO-*b*-PCL-based worm-like micelles (n=6 technical replicates per condition). (D) Concurrently, separate control cells were also treated with the corresponding amounts of PEO_{5k}-PCL_{10k} polymers, using doxorubicin as a negative control. The same oxaliplatin(IV)-loaded PEO-*b*-PCL-based worm-like micelles were used to treat 8988T human pancreatic cancer cells (5,000 cells per well) at comparable doses; and, cellular viability was similarly assessed by the CellTiterGlo assay after (E) 1 day, (F) 2 days, and (G) 3 days after nanoparticle addition. (H) Control cells were similarly treated with the corresponding amounts of PEO_{5k}-PCL_{10k} polymers, using doxorubicin as a negative control. Note that in (D) and (H), NP1, NP2, NP3, NP4 and NP5 correspond to 5.2 mM (78 μg/μL), 2.6 mM (39 μg/μL), 0.52 mM (7.8 μg/μL), 0.26 mM (3.9 μg/μL), and 0.052 mM (0.78 μg/μL) of PEO_{5k}-PCL_{10k} diblock copolymer, respectively.

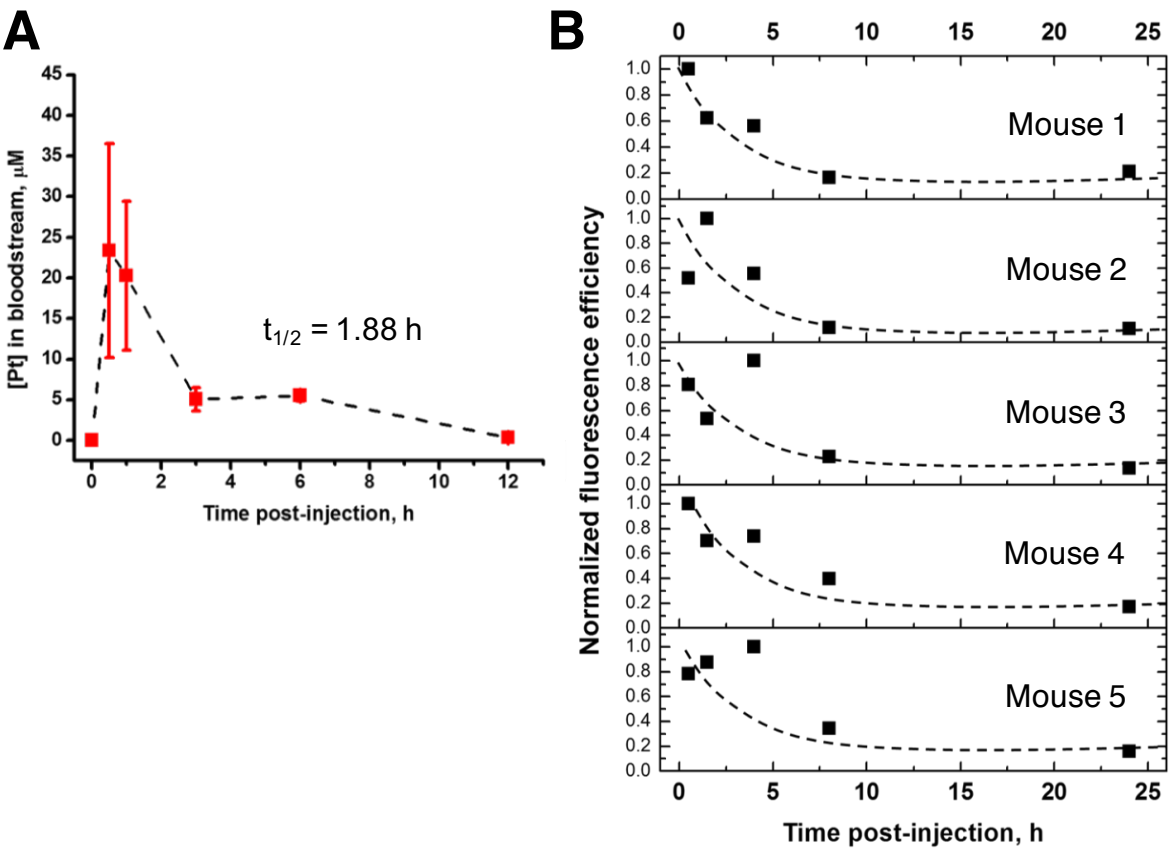

Figure S10. Pharmacokinetics of free oxaliplatin versus DiR-encapsulated and oxaliplatin(IV)-loaded PEO-*b*-PCL-based worm-like micelles as assessed in the SQ murine model of PDAC. (A) Changes in blood Pt concentrations over time (as measured from 0.4-0.5 mL of blood withdrawn by terminal cardiac puncture after euthanasia by CO_2) from mice that were injected with free oxaliplatin (n=4 mice). (B) Changes in the fluorescence radiant efficiency values from mouse blood (15 μL) over time; blood was withdrawn from the retro-orbit of mice that were injected with DiR-encapsulated and oxaliplatin(IV)-loaded PEO-*b*-PCL-based worm-like micelles (n=5 mice). The fluorescence radiant efficiency values in subsequent blood draws were normalized to the highest value obtained from the initial blood draw from the same mouse and were plotted as a function of time post-nanoparticle injection.

SUPPLEMENTAL REFERENCES

[1] Z. Tao, X. Dang, X. Huang, M.D. Muzumdar, E.S. Xu, N.M. Bardhan, H. Song, R. Qi, Y. Yu, T. Li, W. Wei, J. Wyckoff, M.J. Birrer, A.M. Belcher, P.P. Ghoroghchian, Early tumor detection afforded by in vivo imaging of near-infrared II fluorescence, Biomaterials 134 (2017) 202-215.